J|A|C|S
ARTICLES
Published on Web 01/09/2007

A DFT Study on the Mechanism of Phosphodiester Cleavage Mediated by Monozinc Complexes

Yubo Fan and Yi Qin Gao*

Contribution from the Department of Chemistry, Texas A & M University, College Station, Texas 77843-3255

Received August 18, 2006; E-mail: yiqin@mail.chem.tamu.edu

Abstract: Density functional theory (DFT), Tao-Perdew-Staroverov-Scuseria (TPSS), is employed to study the reaction mechanism for the zinc-mediated phosphodiester cleavage reaction. The calculations indicate a general base catalysis mechanism. The flexibility of Zn(II) ion's coordination number (5 and 6) as well as the formation of hydrogen bonds between the coordinating water and the ester are responsible for the trapping (namely, coordinating to the Zn complexes) of the phosphodiester. The hydrogen bonds, between the water, the ester, and the nitrogen-ligand, tris(6-amino-2-pyridylmethyl)amine, not only stabilize the key five-coordinated phosphorus intermediates with a trigonal pyramidal PO_5 unit but also lower the energy barriers for the proton transfer within the complexes by gaining stronger solvation energies.

Introduction

Nature has been using phosphodiesters as linkages between nucleotides in DNA, which stores genetic information for all aspects of lives, because of its exceptional stability against hydrolysis in neutral aqueous solution, with a half-life of 30 000 000 years for hydrolysis of the linkage at 25 °C.[1,2] RNA is not as stable as DNA because of the 2′-OH, which may attack the phosphorus to break the linkage on the pentose; although RNA is stable in neutral environment, because hydroxyl is a weak base comparable to water, the hydroxyl can be deprotonated at basic conditions and can become a much stronger base to cleave the RNA sequence. Many metalloenzymes, especially zinc-containing ones, accelerate the hydrolysis of phosphodiesters, DNA, or RNA by up to 10^{16}-fold at pH $\approx$ 7.[3−5] On the basis of kinetic, spectroscopic, and crystallographic studies, several zinc complexes were synthesized to mimic the active center for phosphodiester hydrolysis and the corresponding collaborations of metal-ligand and to reveal the kinetics and mechanism in living systems.[6−24]

Recently, a mononuclear Zn(II) complex (**I**) has been reported to accelerate the cleavage of 2-hydroxypropyl 4-nitrophenyl phosphate (**A**, a model for RNA linkage), which undergoes intramolecular transesterification to produce propylene phosphate (**B**) in neutral solutions (see Scheme 1), more efficiently than most known dinuclear Zn(II) complexes.[25] Another Zn(II) complex (**II**), without amino groups on the pyridyls, can also catalyze the transesterification, but it reaches its maximum catalytic activity at pH $\approx$ 8.5 while **I** does at pH $\approx$ 7.[25] In addition, at their maximum activities, **I** catalyzes the cleavage with a rate 2−3 orders of magnitude higher than **II**.

On the basis of their experimental observations, Feng et al.[25] proposed a mechanism in which it was suggested that during the first stage of the catalytic reaction the phosphodiester **A** binds to the zinc complexes, replacing the coordinating water molecule. The deprotonation of the hydroxyl in the substrate occurs after the binding and the zinc ion keeps the five coordination and the trigonal bipyramidal geometry in the catalytic cycle. Their conclusion that the water-coordinated complex is the active species is based on the observation that the inhibition constant of the inhibitors (**DMP** and **PP** in Scheme 2) increases as pH increases even when pH is higher than the

(1) Schroeder, G. K.; Lad, C.; Wyman, P.; Williams, N. H.; Wolfenden, R. *Proc. Natl. Acad. Sci. U.S.A.* **2006**, *103*, 4052−4055.
(2) Williams, N. H.; Wyman, P. *Chem. Commun.* **2001**, 1268−1269.
(3) Lipscomb, W. N.; Sträter, N. *Chem. Rev.* **1996**, *96*, 2375−2433.
(4) Sträter, N.; Lipscomb, W. N.; Klabunde, T.; Krebs, B. *Angew. Chem., Int. Ed. Engl.* **1996**, *35*, 2024−2055.
(5) Wilcox, D. E. *Chem. Rev.* **1996**, *96*, 2435−2458.
(6) O'Donoghue, A. M.; Pyun, S. Y.; Yang, M.-Y.; Morrow, J. R.; Richard, J. P. *J. Am. Chem. Soc.* **2006**, *128*, 1615−1621.
(7) Yang, M.-Y.; Iranzo, O.; Richard, J. P.; Morrow, J. R. *J. Am. Chem. Soc.* **2005**, *127*, 1064−1065.
(8) Mancin, F.; Scrimin, P.; Tecilla, P.; Tonellato, U. *Chem. Commun.* **2005**, 2540−2548.
(9) Morrow, J. R.; Iranzo, O. *Curr. Opin. Chem. Biol.* **2004**, *8*, 192−200.
(10) Livieri, M.; Mancin, F.; Tonellato, U.; Chin, J. *Chem. Commun.* **2004**, *24*, 2862−2863.
(11) Iranzo, O.; Terry, E.; Richard, J. P.; Morrow, J. R. *Inorg. Chem.* **2003**, *42*, 7737−7746.
(12) Iranzo, O.; Kovalevsky, A. Y.; Morrow, J. R.; Richard, J. P. *J. Am. Chem. Soc.* **2003**, *125*, 1988−1993.
(13) Forconi, M.; Williams, N. H. *Angew. Chem., Int. Ed.* **2002**, *41*, 849−852.
(14) Aït-Haddou, H.; Sumaoka, J.; Wiskur, S. L.; Folmer-Andersen, J. F.; Anslyn, E. V. *Angew. Chem., Int. Ed.* **2002**, *41*, 4014−4016.
(15) Cowan, J. A. *Curr. Opin. Chem. Biol.* **2001**, *5*, 634−642.
(16) Molenveld, P.; Engbersen, J. F. J.; Reinhoudt, D. N. *Chem. Soc. Rev.* **2000**, *29*, 75−86.
(17) Krämer, R. *Coord. Chem. Rev.* **1999**, *182*, 243−261.
(18) Wall, M.; Linkletter, B.; Williams, D.; Lebuis, A.-M.; Hynes, R. C.; Chin, J. *J. Am. Chem. Soc.* **1999**, *121*, 4710−4711.
(19) Rossi, P.; Felluga, F.; Tecilla, P.; Formaggio, F.; Crisma, M.; Toniolo, C.; Scrimin, P. *J. Am. Chem. Soc.* **1999**, *121*, 6948−6949.
(20) Williams, N. H.; Takasaki, B.; Wall, M.; Chin, J. *Acc. Chem. Res.* **1999**, *32*, 485−493.
(21) Komiyama, M.; Sumaoka, J. *Curr. Opin. Chem. Biol.* **1998**, *2*, 751−757.
(22) Hegg, E. L.; Burstyn, J. N. *Coord. Chem. Rev.* **1998**, *173*, 133−165.
(23) Chin, J. *Curr. Opin. Chem. Biol.* **1997**, *1*, 514−251.
(24) Kövári, E.; Krämer, R. *J. Am. Chem. Soc.* **1996**, *118*, 12704−12709.
(25) Feng, G.; Mareque-Rivas, J. C.; de Rosales, R. T. M.; Williams, N. H. *J. Am. Chem. Soc.* **2005**, *127*, 13470−13471.

Scheme 1

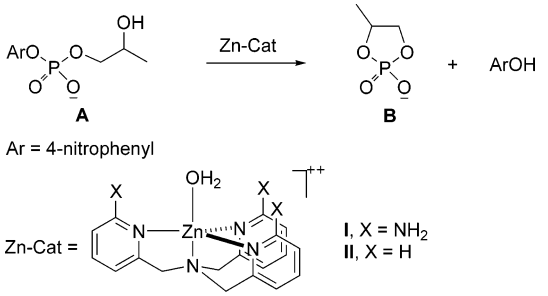

Scheme 2

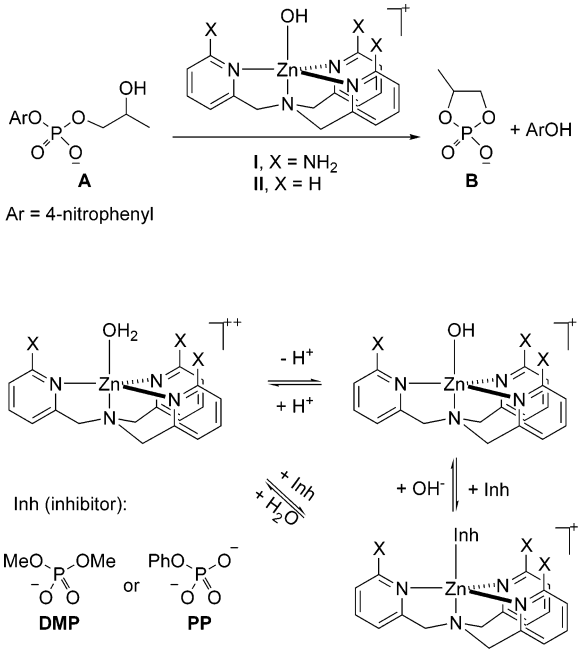

pK_a values of coordinating water in the catalysts. However, this pH dependence of the inhibition constant can also be explained if hydroxo zinc complexes are the active form: because of the competition between Zn−OH (the hydroxo form) and Zn−I (the inhibited form), even at high pH where [Zn−OH_2] (concentration of the aqua form) is negligible, the inhibition effects of **I** decrease with the increase of [OH^-].

Given the experimental observations of Feng et al.,[25] a detailed understanding of the catalytic mechanism is still missing and the involved intermediates and transition states have not been revealed. For example, in the catalysis, does the zinc ion change the coordination and geometry? Does there exist a five-coordinated phosphorus intermediate? How does the proton transfer from the hydroxyl to the 4-nitrophenylate through the hydrogen-bond network in the adducts? Also, more interestingly, what effects make **I** a more effective catalyst than **II**? We hope that by performing an extensive density functional study answers to these mechanistic questions can be found.

Computational Details

The theoretical calculations were carried out using the Gaussian 03[26] implementation of Tao-Perdew-Staroverov-Scuseria (TPSS)[27] density functional theory (DFT). As a new generation of density functional, TPSS matches or exceeds in accuracy almost all prior functionals, including the most popular functional-B3LYP.[28]

The basis sets for zinc and phosphorus were Stuttgart/Dresden (SDD) with the effective core potential (ECP)[29] and LANL2DZ plus a *d*-polarization and a *p*-diffuse function[30] with ECP,[31,32] respectively. 6-31++G(d′,p′) basis sets were used for C, N, O, and all H atoms bound to N and O,[33−35] while 6-31G was used for the rest of all H atoms.[33] In addition, density fitting functions were included to accelerate the computation with DFT.[36,37] Density fitting functions can be included for this pure DFT, and only pure DFT, to save tremendous computational expense by expanding the density in a set of atom-centered functions when computing the Coulomb interaction instead of computing all of the two-electron integrals.[36,37] A comparison of TPSS with or without density fitting functions included for an organometallic reaction shows only marginal difference for both relative energies and structural parameters.[38] TPSS reproduces their properties at least as precisely as B3LYP. Especially, TPSS can recognize relatively weak interactions (such as agostic interactions) very well while B3LYP significantly underestimates them.[38] Furthermore, using smaller basis sets for the atoms far from the reaction center does not degrade the computational precision and accuracy significantly but can accelerate the calculations considerably.[38]

All structures were fully optimized and frequency analyses were performed to ensure a minimum or transition state was achieved. Furthermore, all transition states were confirmed with the intrinsic reaction coordinate (IRC) method[39,40] to connect to the corresponding reactants and products. The thermodynamic functions, including enthalpies, entropies, and free energies, were calculated at 298.15 K and 1 atm. The solvation energies for all species in aqueous solution were estimated with the polarizable continuum model (PCM).[41]

Results and Discussion

In principle, there could be multiple pathways in forming a reactive complex−catalyst−substrate adduct, which, for example, can be formed by either Zn−OH + **A**, as given in the present paper as the favored mechanism, or by Zn−OH_2 + $\mathbf{A}^-$ with a subsequent proton transfer (**A** and $\mathbf{A}^-$ are the substrate and its deprotonated form shown in Scheme 3). However, the big difference between the pK_a values of Zn−OH_2 and substrate **A** suggests that the former pathway is much more likely.

In the case of catalyst **I**, at pH of 7−12 (pK_a of 6.0[42] for **I** and pK_a of ∼13[43,44] for the hydroxyl in **A**), both the products of concentrations, [Zn−OH_2][$\mathbf{A}^-$] and [Zn−OH][**A**] although the ratio between them, [Zn−OH_2][$\mathbf{A}^-$]/[Zn−OH][**A**], equals

(26) Frisch, M. J. et al. *Gaussian 03*, Revision B.4, B.5, and C.1; Gaussian, Inc.: Pittsburgh, PA, 2003.
(27) Tao, J.; Perdew, J. P.; Staroverov, V. N.; Scuseria, G. E. *Phys. Rev. Lett.* **2003**, *91*, 146401-1−146401-4.
(28) Staroverov, V. N.; Scuseria, G. El; Tao, J. M.; Perdew, J. P. J. *Chem. Phys.* **2003**, *119*, 12129−12137.
(29) Dolg, M.; Wedig, U.; Stoll, H.; Preuss, H. *J. Chem. Phys.* **1987**, *86*, 866−872.
(30) Check, C. E.; Faust, T. O.; Bailey, J. M.; Wright, B. J.; Gilbert, T. M.; Sunderlin, L. S. *J. Phys. Chem. A* **2001**, *105*, 8111−8116.
(31) Hay, P. J.; Wadt, W. R. *J. Chem. Phys.* **1985**, *82*, 270−283.
(32) Hay, P. J.; Wadt, W. R. *J. Chem. Phys.* **1985**, *82*, 284−398.
(33) Hehre, W. J.; Ditchfield, R.; Pople, J. A. *J. Chem. Phys.* **1972**, *56*, 2257−2261.
(34) Clark, T.; Chandrasekhar, J.; Spitznagel, G. W.; Schleyer, P. von R. *J. Comput. Chem.* **1983**, *4*, 294−301.
(35) Krishnan, R.; Binkley, J. S.; Seeger, R.; Pople, J. A. *J. Chem. Phys.* **1980**, *72*, 650−654.
(36) Dunlap, B. I. *J. Chem. Phys.* **1983**, *78*, 3140−3142.
(37) Dunlap, B. I. *J. Mol. Struct. Theochem.* **2000**, *529*, 37−40.
(38) Fan, Y.; Hall, M. B. *Organometallics* **2005**, *24*, 3827−3835.
(39) Gonzalez, C.; Schlegel, H. B. *J. Chem. Phys.* **1989**, *90*, 2154−2161.
(40) Gonzalez, C.; Schlegel, H. B. *J. Phys. Chem.* **1990**, *94*, 5523−5527.
(41) Cossi, M.; Scalmani, G.; Rega, N.; Barone, V. *J. Chem. Phys.* **2002**, *117*, 43−54.
(42) Mareque-Rivas, J. C.; Prabaharan, R.; de Rosales, R. T. M. *Chem. Commun.* **2004**, 76−77.
(43) Lönnberg, H.; Strömberg, R.; Williams, A. *Org. Biomol. Chem.* **2004**, *2*, 2165−2167.
(44) Velikyan, I.; Acharya, S.; Trifonova, A.; Foeldesi, A.; Chattopadhyaya, J. *J. Am. Chem. Soc.* **2001**, *123*, 2893−2894.

Scheme 3

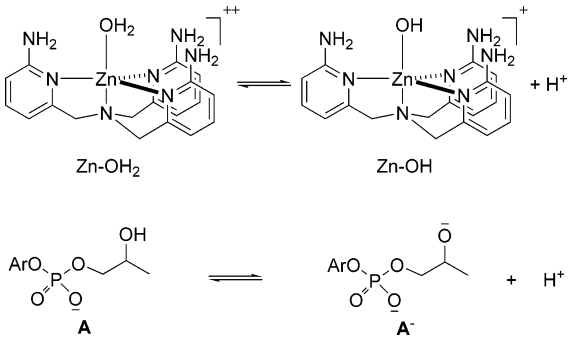

Scheme 4

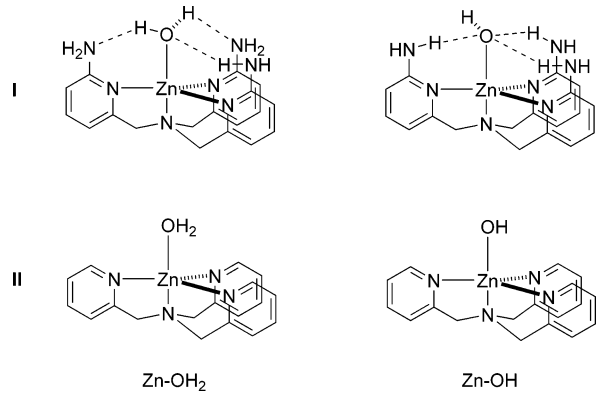

10^{-7}, are largely pH independent. However, this invariance for the aqua form of **I** is resulted from the simultaneous decrease of [Zn−OH_2] and increase of [$\mathbf{A}^-$] along the increase of pH while that for the hydroxo is from that both the Zn−OH and **A** are the dominating forms for the catalyst and substrate, respectively. Thus, both the aqua and the hydroxo forms of the catalysts present the same kinetics for the binding and cleavage in the experiment. Namely, they are kinetically identical in the pH-rate profile.[25] To focus the investigation on the catalysis after binding, the hydroxo Zn(II) complexes and hydroxyl form of the substrate **A** were calculated for the catalytic mechanism as they are dominating species under the optimal conditions, although more experiments, especially kinetic studies on the pH dependence of binding of different substrate forms, are needed to distinguish among different pathways.

Structures of the Aqua- and Hydroxo-Coordinating Catalysts. The geometry optimization, for protonated and deprotonated forms of the five-coordinated Zn complexes, indicates that both forms keep trigonal bipyramyl geometry before the substrate binding (see Scheme 4). In the structure of the aqua catalyst **I**, the two protons on the water form two hydrogen bonds with two amino groups on the ligand while the third amino forms a hydrogen bond with the water oxygen. The three N−Zn−N bond angles in the equatorial plane are virtually identical, ranging from 111.4° to 118.7°. In contrast, in the hydroxo form, the hydroxo oxygen forms a hydrogen bond with each of the three aminos while the hydroxo proton does not interact with the N-ligand. The equatorial N−Zn−N bond angles diverge to two groups: on the free hydroxo proton side, the bond angle is 126.4°; the other two are nearly the same, 109.9° and 111.4°. The structural characteristics further prove that the hydroxo form is a better catalyst since the substrate **A** can coordinate to Zn from the more open site and form hydrogen bonds with the coordinating hydroxyl and the amino group simultaneously. Differently, the aqua form has to adjust its geometry, even to break or to switch some hydrogen bonds, to stably bind the substrate. For the simpler version catalyst **II**, the geometries are quite symmetric, lacking interactions between the N-ligand and the coordinating water/hydroxide.

Catalysis with I. As the mechanism and the structures shown in Scheme 5 and Figures 1and 2, respectively, substrate **A** binds to Zn to form a six-coordinated complex (**1**) with an octahedral geometry instead of the trigonal bipyramidal in catalyst **I** without substrate (see Scheme 4) while three hydrogen bonds, O2−H5···N5, O1−H1···O5, and N6−H3···O5 in Figure 1, form between them to enhance the binding. As a result, the hydroxyl is held close to the tetrahedral phosphorus and is ready to attack. **TS-2** in Figure 1 is the transition state for the attacking of O2 against the phosphorus atom to form the five-coordinated phosphorus intermediate **3a**. In this transition state, the fifth P−O bond is forming (P−O2 is 2.161 Å), H5 is exchanging between O2 and N5, and H2 has already transferred to the coordinating hydroxide to form water. These two proton-transfer reactions apparently increase the basicity of the hydroxyl on **A** and also deliver away the accumulated positive charge on the oxygen atom when the P−O bond is forming. **3a** is the formed intermediate with the five-coordinated phosphorus bound to the ligands by three hydrogen bonds. In another intermediate, **3b**, the hydrogen bonds involving the water are between O5 and H2 and between N6 and H2. **TS-4a** is the transition state between **3a** and **3b**, in which H2 interacts with both O2 and O5, for the rotation of the coordinating water by Zn−O1 bond to form **3b**. Subsequently, the hydrogen bond between O2 and H5 is broken to form another one between O1 and H5 as in **3c**. In **TS-4b**, H5 is switching hydrogen bond from O2 to O1 while H2 transfers from O1 to O5 to lower the positive and negative charge densities on the coordinating water and the PO_5 unit, respectively, caused by the forming hydrogen bond between O1 and H5. The breaking of the hydrogen bond between O2 and H5 also enhances the interactions between O3 and H3 although it is a very weak hydrogen bond as seen from the long distance of 2.8 Å in **3c**. Driven by the formation of this weak hydrogen bond, the entire PO_5 unit rotates by the P−O6 bond. Via transition-state **TS-4c**, another intermediate **3d**, with two hydrogen bonds to O3, forms. These two hydrogen bonds significantly weaken P−O3 bond, which is elongated from 1.83 to 1.86 Å (**3a**−**c**) to 2.0 Å (**3d**). After this P−O bond is broken, the products, cyclic phosphodiester **B** and 4-nitrophenylate, form, although they are still bound to Zn(II) ion and the ligands in **6**. The proposed transition-state **TS-5**, between **3d** and **6**, was not located because of the weak P−O3 bond. As long as any stronger interactions were introduced, such as that because of the shortening of the O3−H1 or O3−H3 distance, the P−O3 bond breaks spontaneously according to our optimizations of geometry and scanning of potential energy surface (PES). The barrier for this bond-breaking is too low to be observed at the theoretical level we employed.

The relative free energies along the reaction pathway shown in Scheme 5 are listed in Table 1. In the gas phase, the highest energy species is the transition-state **TS-4a** for the rotation of the coordinating water, and the overall activation free energy is 22.7 kcal/mol. The barrier decreases to 14.7 kcal/mol when the solvation energies in water solution are included and all

Scheme 5

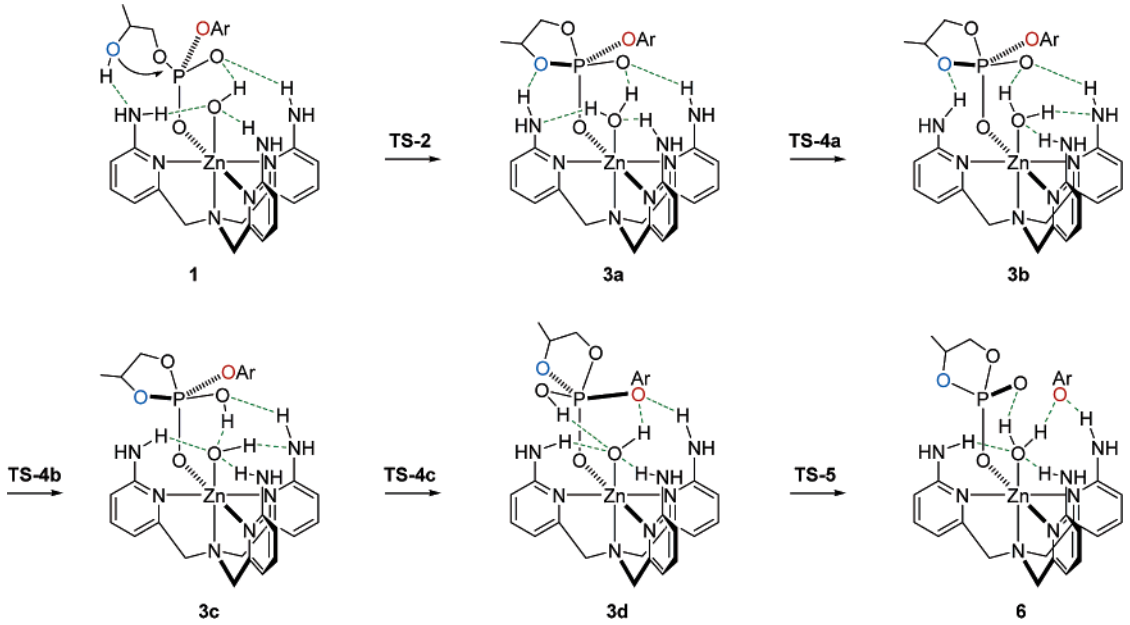

transition states and intermediates are stabilized significantly. Interestingly, **3a** is more stable than **3b** by about 5 kcal/mol although they have the same number and the same type of hydrogen bonds. The difference between **3a** and **3b** is that the coordinating water switches the hydrogen bond from O1−H2−N5 in the former to O1−H1−N6 in the latter. The relative instability of **3b** is primarily resulted from the more restrained triangular hydrogen-bond network of O1, O5, and N6. The tetrahedral geometry of O−H bonds and lone pairs of electrons in the coordinating water limits the orientations of the hydrogen bonds and weakens the hydrogen bonds between O1 and N6 and between O1 and N7. The distances between N6 and H1 and between O1 and H4 are significantly elongated, 2.089 Å and 1.890 Å versus 1.917 Å (N5−H2 instead) and 1.761 Å in **3b** and **3a**, respectively. Strikingly, five species (**TS-4a**, **3b**, **TS-4b**, **3c**, and **TS-4c**) are nearly isoenergetic, indicating that this proton-transfer process is highly stabilized by the hydrogen-bond network (see Figure 1) formed in these species.

Catalysis with II. The mechanism for catalyst **II** is shown in Scheme 6, and the structures for all species involved are depicted in Figure 2. The mechanism shown in Scheme 6 is much simpler than that for catalyst **I**, primarily because of the lack of a hydrogen-bond network in the absence of the amino groups. The substrate **A** binds to the zinc complex by coordinating one of the phosphate oxygen atoms to zinc and forming two hydrogen bonds between O1 and H2 and between O4 and H1 (**1′** in Figure 2). The latter hydrogen bond is relatively weak given that the distance between O4 and H1 is 2.8 Å. In addition, an even weaker hydrogen bond exists between O5 and H1 with a distance of 3.1 Å. Via transition-state **TS-2′**, in which the P−O2 is a forming bond with a distance of 2.23 Å, a five-coordinated phosphorus intermediate **3′a** forms with proton H2 transferred from O2 to O1 to form a water molecule bound to zinc instead of hydroxide in **1′**. Also, there are two hydrogen bonds between O2 and H2 and between O5 and H1. **TS-4′** is the transition state for the rotation of the coordinating water. The hydrogen bond between O5 and H1 is already broken and H2 is moving and switching the hydrogen bond with O2 to a new one toward O5. **3′b**, also including a PO_5 unit, is the intermediate following the rotation of water. The intrinsic reaction coordinate (IRC) calculations for **TS-4′** indicate the direct connection between **3′a** and **TS-4′** and between **3′b** and **TS-4′**. The formed hydrogen bond between O5 and H2 further leads the PO_5 unit to rotate by the P−O6 bond. After this rotation, a weak hydrogen bond forms between O3 and H1 with a distance of 2.7 Å and proton H2 transfers to O5. In **3′b**, the P−O3 bond is elongated by about 0.04 Å relative to **3′a**. **TS-5′** is the transition state for the breaking of the P−O3 bond. In this structure, the 4-nitrophenolate is about to leave with a long P−O3 bond of 2.17 Å while the hydrogen bond between O3 and H1 has become stronger and proton H2 is migrating back to form a water molecule coordinating to zinc. After this cleavage, **6′** forms with the cyclic phosphodiester **B**, bound to zinc with a coordination bond and a hydrogen bond, and the 4-nitrophenylate, one of the products, forms a hydrogen bond to the coordinating water.

In Table 2, the relative free energies are listed for the mechanism shown in Scheme 6. Similar to catalyst **I**, the transition-state **TS-4′** is the species with the highest energy along the reaction pathway and the overall activation free energy is 22.7 kcal/mol in gas phase. The barrier decreases to 18.0 kcal/mol when the solvation energies are taken into account.

Reaction Paths without the Coordinating Water or Hydroxide As a possible reaction path, the substitution mechanism proposed by Feng et al.[25] for catalyst **I** was also calculated for comparison. Instead of forming a five-coordinated complex as suggested by Feng et al.,[25] the calculations show that when substrate **A** replaces the coordinating water, a six-coordinated complex is formed. Although several different conformations were found, cation **7** shown in Scheme 7 was located as the most stable one. We also tried to search the five-coordinated form with the phosphate oxygen or the hydroxyl oxygen but the optimization always resulted in six-coordinated structures. In Scheme 7, **8** is the conjugate base of **7** by deprotonation. Removing proton from the coordinating hydroxyl in other

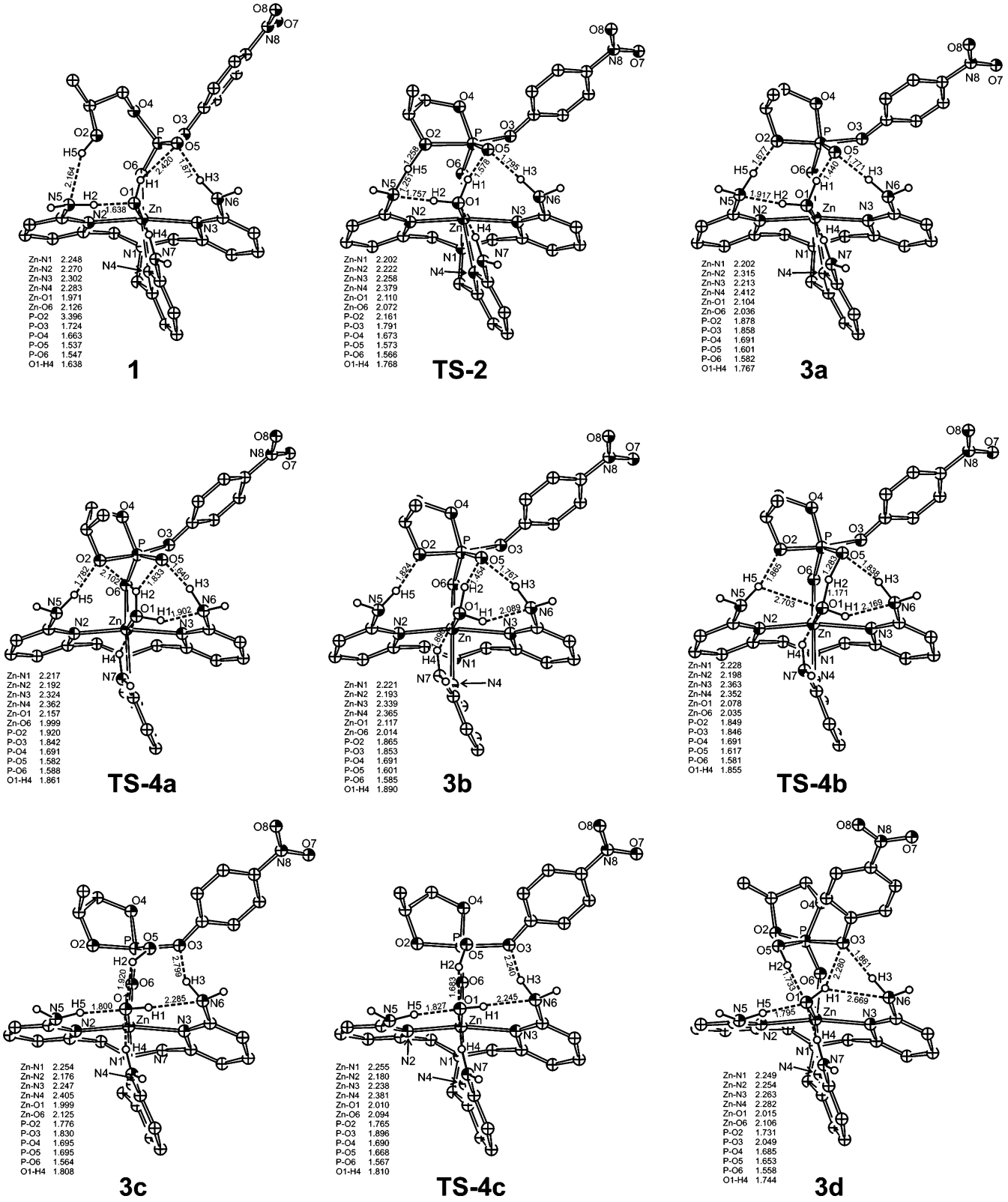

Figure 1. Optimized structures for the mechanism shown in Scheme 3. Hydrogen atoms on carbons are omitted for clarity. The distances are in Å.

conformations of **7** all results in **8**. **9** and **10** are the five-coordinated phosphorus intermediates for the attacking of the deprotonated hydroxyl oxygen in **8** against the phosphorus atom. Because of the strain of the four-member ring and the steric effects between the propylene group and the ligand in **9**, **10** was located even structure **9** was used as the initial geometry for the optimization.

Since the transition state was not found between **8** and **10**, the potential energy surface (PES) along the distance between the attacking oxygen and the phosphorus was carefully scanned.

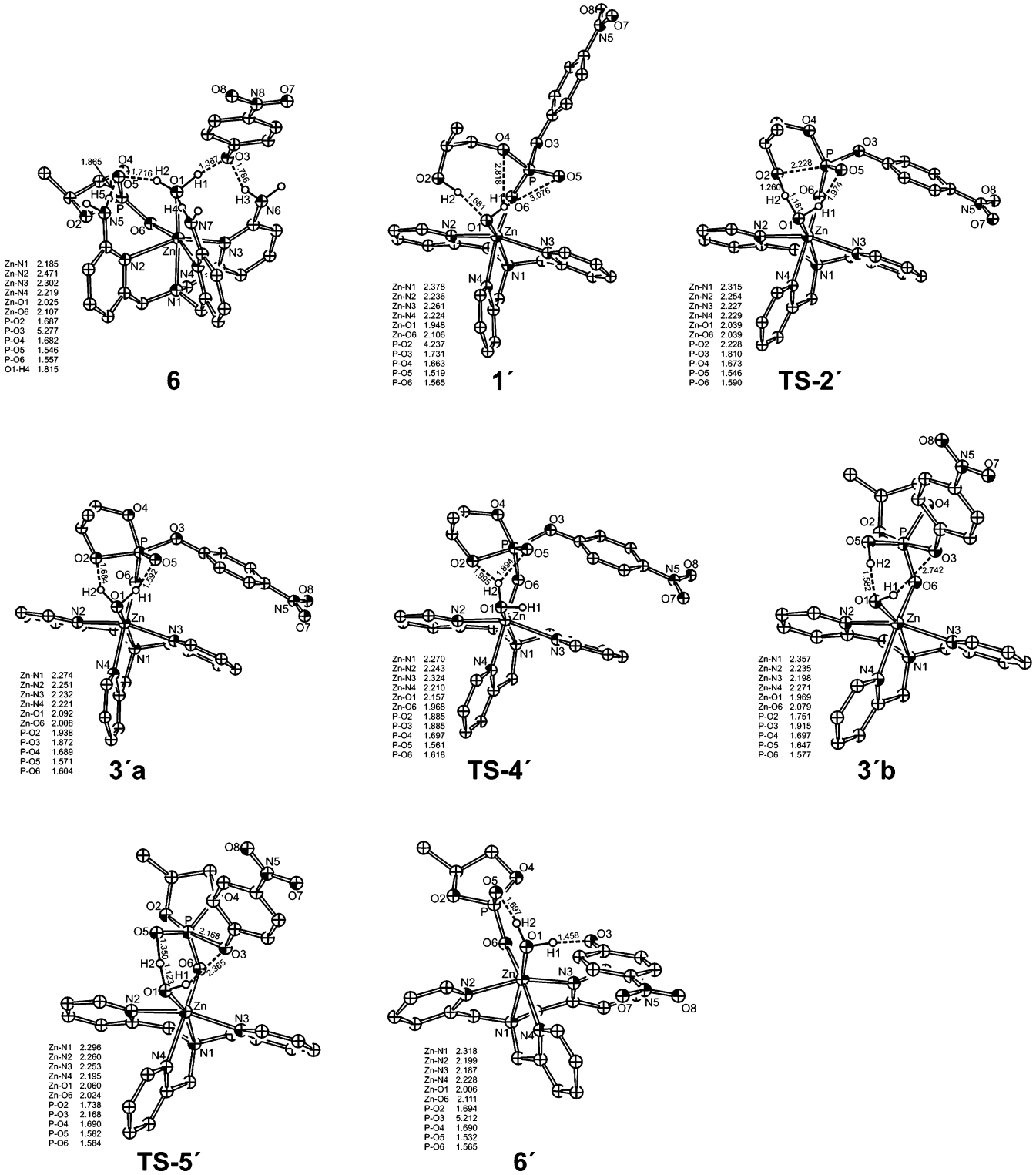

Figure 2. Optimized structures for the mechanism shown in Schemes 3 and 4. Hydrogen atoms on carbons are omitted for clarity. The distances are in Å.

Table 1. The Relative Free Energy in Gas-Phase ΔG and in Water Solution ΔG_s (kcal/mol) for the Catalytic Cycles with Catalyst **I**

	1	TS-2	3a	TS-4a	3b	TS-4b	3c	TS-4c	3d	TS-5	6
ΔG	0.00	17.81	16.36	22.70	21.10	20.05	15.63	18.62	12.79		−6.81
ΔG_s	0.00	13.82	8.74	14.72	13.82	13.62	13.65	14.63	9.47		−11.76

Although the scanning was not exhausted, the calculations showed that the Zn−O bond must break before the oxygen can attack the phosphorus if the proposed transition state exists. Namely, losing a Zn−O bond without forming a P−O bond simultaneously leads to a state with a high energy. The PES scan shows that the barrier for this reaction path is at least 18 kcal/mol if the transition state exists. Furthermore, since the orientation of the leaving group, 4-nitrophenoxyl, is confined

Scheme 6

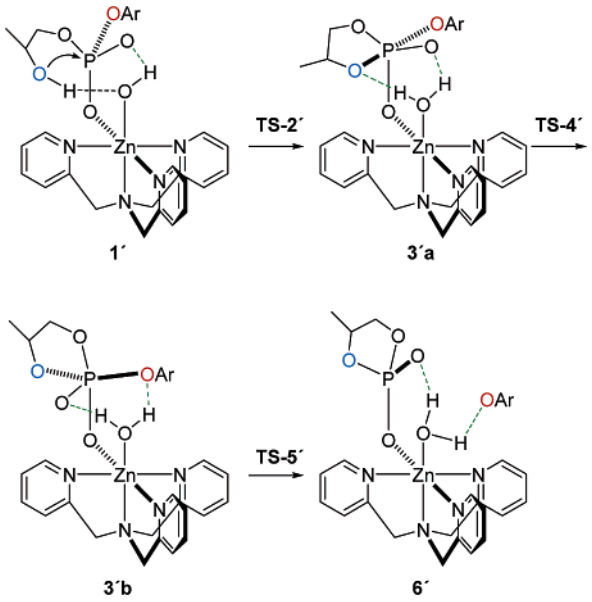

by the restraint of the coordinating deprotonated hydroxyl, the proton from the hydroxyl is unable to be delivered to the leaving group through the hydrogeon-bond network in the adduct. Instead, the proton is dissolved into the solvent. Thus, this reaction path, if it exists, is disfavored compared to the one with hydroxide included shown above.

Coordination of Catalysts I and II. The flexibility of Zn(II) ion's coordination numbers provides stable active catalysts with coordination of five and adducts with coordination of six. Exploring X-ray crystal data for Zn complexes with a tetradentate N-ligand similar to those in catalyst **I** or **II**, it is found that trigonal bipyramidal geometry (five-coordination) is favored by Zn with a monodentate ligand, such as halides and hydroxide,[45−47] while octahedral (six-coordination) is preferred with a bidentate ligand.[48,49] Surprisingly, when the second ligand is nitrate, the coordination is already changed to an intermediate between trigonal bipyramidal and octahedral. One N−Zn−N (N atoms on the pyridyl groups) bond angle increases to 140.1° [50] from 112.0 to 121.1° in chloride-coordinated complexes[45,46] while the other two decrease to 101.3° and 109.7°, respectively.[50] The nitrate has a second O coordinating to Zn from the more open site although the bond length is 2.64−2.85 Å relative to 2.04−2.10 Å for the stronger Zn−O bond. Apparently, the coordination is determined by entropy so that changing from coordination of five to six is only a matter of several kcal/mol. Such a low-energy change will not be an obstacle for the catalysts to capture substrate **A** without losing the hydroxide in the catalytic cycle.

Acidity of the Coordinating Water. In principle, the possibility cannot be ruled out that the pK_a of the coordinating water in the protonated form of **1** (in Scheme 5) is high enough to be outside the range (pH = 5.5−10.5) in the experiment, since Zn changes coordinate from five to six after the anionic substrate binding. However, deprotonation of this water is critical for the catalytic activity because only the coordinating hydroxide, not water, is basic enough to position the hydroxyl ready to attack and to increase its basicity by forming hydrogen bonds. In the case of catalyst **I** (**II** is similar), since no pH-dependence is observed at pH above the catalyst's pK_a (=6.0), it is very likely that the pK_a of the coordinating water in the six-coordinated complex is close to the catalyst's and that the hydroxo form is the catalytic form. Furthermore, the atomic partial charge calculations also support the similar basicity of the hydroxide in the hydroxo form of **I** and **1** although estimating pK_a is still a challenge in computational chemistry.[51]

Table 2. The Relative Free Energy in Gas-Phase ΔG and in Water Solution ΔG_s (kcal/mol) for the Catalytic Cycles with Catalyst **II**

	1	**TS**-2	**3**a	**TS**-4	**3**b	**TS**-5	**6**
ΔG	0.00	14.88	14.67	22.70	10.86	12.11	−15.56
ΔG_s	0.00	16.47	14.15	18.01	10.81	8.06	−17.63

Inhibition. The inhibitors, DMP and PP in Scheme 2, bind to catalysts to form five-coordinated adducts, likely through six-coordinated intermediates. In the case of DMP with catalyst **I**, compared to **1** in Scheme 5, the adduct between Zn−OH and DMP (Zn−OH−DMP) has one less hydrogen bond, which costs several kcal/mol and likely switches the relative stability between five- and six-coordinated species. Thus, the coordinating water or hydroxide tends to dissociate into the solvent to reform a five-coordinated complex. Apparently, the inhibitors lower the concentration of the active form of the catalyst and result in drops of the catalytic activity. On the other hand, as the equilibrium shown in Scheme 2, increasing pH certainly increases the concentration of the hydroxo form of catalyst **I** and the concentration of **1**. Namely, high pHs suppress the inhibition and accelerates the catalysis.

Leaving Groups. Although substrate **A**, 2-hydroxypropyl 4-nitrophenyl phosphate, is widely used as a model for RNA linkage to estimate the activity of catalysts in experiments, the cleaved bond is a phenoxyl-phosphorus bond while it is an alkoxyl-phosphorus (5′-hydroxyl) bond in RNA. Because of the tremendous difference between pK_as of 4-nitrophenol and the 5′-hydroxyl in nucleotides (7.15 vs ∼15, which is estimated from 15.5 of ethanol, 15.1 of ethylene glycol, and 14.15 of glycerol[52]), the phenol could leave as a basic form under neutral conditions while the alkyl one only does so as an alcohol.[43,53,54] However, in the mechanism shown in Scheme 2, a proton is transferred from the substrate hydroxyl to the leaving phenolate although it is only hydrogen-bonded to the phenolate. If the leaving group is an alcohol, the P−O bond cleavage would be an analogue to the reverse process of the P−O formation in the first step. Thus, the relative free energy of the transition state,

(45) Mareque-Rivas, J. C.; Salvagni, E.; de Rosales, R. T. M.; Parsons, S. *Dalton Trans.* **2003**, 3339−3349.
(46) Mareque-Rivas, J. C.; Prabaharan, R.; de Rosales, R. T. M.; Metteau, L; Parsons, S. *Dalton Trans.* **2004**, 2800−2807.
(47) Mareque-Rivas, J. C.; Prabaharan, R.; Parsons, S. *Dalton Trans.* **2004**, 1648−1655.
(48) Makowska-Grzyska, M. M.; Szajna, E.; Shipley, C.; Arif, A. M.; Mitchell, M. H.; Halfen, J. A.; Berreau, L. M. *Inorg. Chem.* **2003**, *42*, 7472−7488.
(49) Wada, A.; Yamaguchi, S.; Jitsukawa, K.; Masuda, H. *Angew. Chem., Int. Ed.* **2005**, *44*, 5698−5701.
(50) Mareque-Rivas, J. C.; de Rosales, R. T. M.; Parsons, S. *Chem. Commun.* **2004**, 610−611.
(51) The atomic partial charges on Zn and the coordinating O are 1.33 and −0.76 e$^-$, respectively, in **I** and 1.58 and −0.74 e$^-$, respectively, in **1** using generalized atomic polar tensor (GAPT) charge method. Cioslowski, J. *J. Am. Chem. Soc.* **1989**, *111*, 8333−8336.
(52) Lide, D. R. *CRC Handbook Chemistry and Physics*, 85th Ed.; CRC-Press: Boca Rton, FL, 2004.
(53) Mikkola, S.; Stenman, E.; Nurmi, K.; Yousefi-Salakdeh, E.; Strömberg, R.; Lönnberg, H. *J. Chem. Soc., Perkin Trans. 2* **1999**, 1619−1625.
(54) Komiyama, M.; Matsumoto, Y.; Takahashi, H.; Shiiba, T.; Tsuzuki, H.; Yajima, H.; Yashiro, M.; Sumaoka, J. *J. Chem. Soc., Perkin Trans. 2* **1998**, 691−695.

Scheme 7

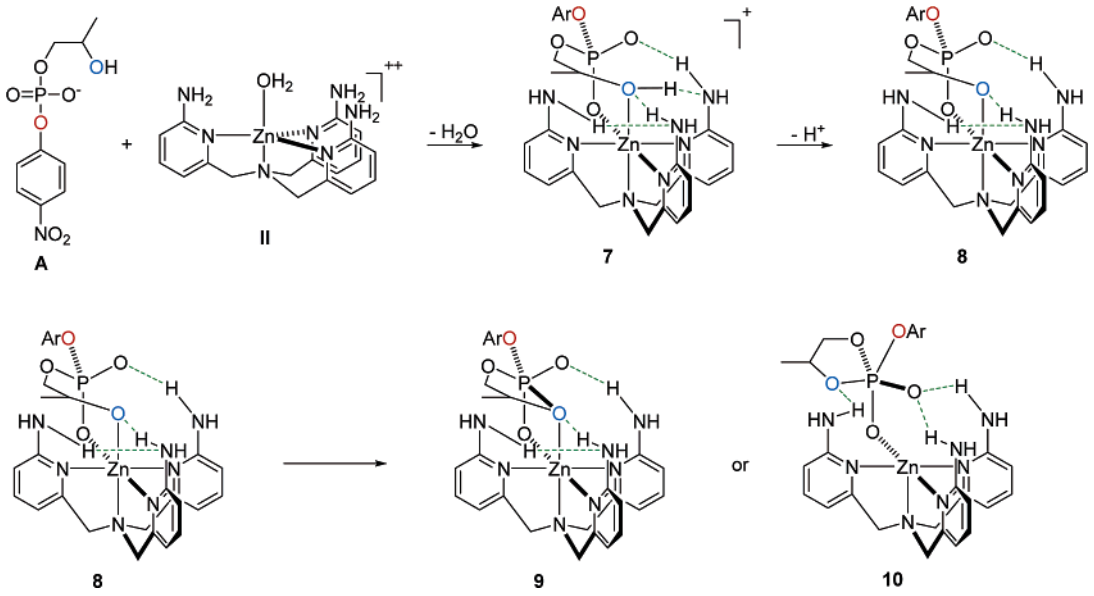

in which a proton on the coordinating water is already hydrogen-bonded to the leaving oxyanion, for this step is expected to be similar to that for the P−O bond formation. Since the relative free energies (see Table 1) of the transition states shown in Figure 1 are close, introducing a strong electronic effect could possibly change the order of the energies. Namely, the rate-determining step in the cleavage of the linkage between nucleotides could be different from what we proposed for the model substrate **A**.

Conclusions

Our calculations revealed a reasonable reaction pathway for the Zn-catalyzed cleavage of phosphodiester, the coordination and hydrogen-bonding situations in the catalytic cycle, which is different from what has been suggested earlier.[25] The results indicate a general base catalysis, which was also observed in the kinetics of a dizinc complex-mediated phosphodiester cleavage,[7] and the mechanisms for these two catalysts are overall similar, although their maximum catalytic activities differ by 2−3 orders of magnitude. Substrate **A** binds to zinc complexes by coordinating to Zn and by hydrogen-bonding to the ligands. While the hydroxyl on **A** attacks the phosphorus, the proton of the hydroxyl transfers to the coordinating hydroxide to enhance basicity of the hydroxyl and to remove the accumulated positive charge from the oxygen. Not surprisingly, all five-coordinated phosphorus intermediates possess much higher energy than the tetrahedral phosphate adducts in these two mechanisms. Before the cleavage between the phosphorus and the 4-nitrophenylate occurs, the coordinating water rotates and forms a relatively weak hydrogen bond to the phenylate oxygen. This hydrogen bond significantly weakens the corresponding P−O bond and the following breaking of the latter is almost barrierless.

These two Zn complexes (**I** and **II**) provide an excellent metal-ligand collabration model for RNA hydrolysis mediated by metalloenzymes. The stability of the five-coordination of Zn(II) maximizes the concentration of the active catalyst, which is different from most other catalysts that dissociate and drive one ligand off to empty one coordination for substrates. The slight instability of the six-coordination of Zn(II) permits fast product release as soon as they are formed.

The mechanisms of the two catalysts (**I** and **II**) are quite similar and the rotation of the coordinating water is the rate-determining step. Apparently, primary isotope effect might be observed if the coordinating water is deuterated. The overall free-energy barriers are almost identical in gas phase for these two catalysts. However, once solvent effects are introduced, the reaction catalyzed by **I** has a lower barrier. The calculated free-energy barrier for the reaction catalyzed by **I** is 3.3 kcal/mol lower that that by **II**, which is consistent to the corresponding experimental value of 2.6 kcal/mol estimated from the ratio between the limiting rate constants (a 79-fold difference between the reaction catalyzed by catalysts **I** and **II**).[25,55] Actually, in the mechanism of catalyst **II**, the solvation free energies are fairly constant for all species. However, in the case of catalyst **I**, the solvent stabilizes the intermediates (**3a**−**c**) and transition states (**TS-2** and **TS4a**−**c**) more than the reactant-bound adduct **1′** by 4∼8 kcal/mol because the hydrogen-bond network in **I**-mediated catalysis provides extra solvation energies for these species including PO_5 unit. In contrast, in the case of catalyst **II**, the solvent effects only contribute 2∼4 kcal/mol.

As a trend, the more amino groups exist in the N-ligand, the more acidic the coordinating water is,[42] and the more solvation energies can be gained to stabilize the intermediates and transition states and the more flexibly the proton transfers from the substrate hydroxyl to the leaving group or more basic species in the reaction system. Predictably, catalyst **I** and **II** reach their maximum activity at the lowest and highest pH, respectively. The mono- and diamino-substituted catalysts reach the maximum in-between. Similarly, catalyst **I** is the most active catalyst and **II** is the least at their optimal pHs while monoamino and diamino species are again in-between.

(55) The estimated value in the experiment is 3.9 kcal/mol by assuming that the binding affinity of the substrate is the same as the inhibitor DMP. Apparently, this assumption is different from the favored mechanism we calculated. DMP binds to the catalysts and replaces the coordinating water or hydroxide while the substrate **A** binds with water or hydroxide still kept.

Acknowledgment. We would like to thank the Welch Foundation for their generous support. We also appreciate the computation supports from the supercomputer facilities in the Department of Chemistry and Texas A & M University (NSF-DMS 0216275). Y.Q.G. is a 2006 Searle Scholar. We thank anonymous reviewers for their helpful comments and suggestions.

Supporting Information Available: Cartesian coordinates (in Å), electronic energies, zero-point energies, enthalpies, free energies (in Hartree), and solvation free energies (in kcal/mol) for all species included in Figures 1 and 2 and complete ref 26. This materials is available free of charge via the Internet at http://pubs.acs.org.

JA0660251